Nanoscale

PAPER

Cite this: *Nanoscale*, 2017, **9**, 5244

Interface engineering for a rational design of poison-free bimetallic CO oxidation catalysts†

Kihyun Shin,‡[a] Liang Zhang, §‡[b] Hyesung An,[c] Hyunwoo Ha,[c] Mi Yoo,[c] Hyuck Mo Lee,[a] Graeme Henkelman[b] and Hyun You Kim *[c]

Received 24th February 2017,
Accepted 17th March 2017

DOI: 10.1039/c7nr01382e

rsc.li/nanoscale

We use density functional theory calculations of Pt@Cu core@shell nanoparticles (NPs) to design bifunctional poison-free CO oxidation catalysts. By calculating the adsorption chemistry under CO oxidation conditions, we find that the Pt@Cu NPs will be active for CO oxidation with resistance to CO-poisoning. The CO oxidation pathway at the Pt–Cu interface is determined on the Pt NP covered with a full- and partial-shell of Cu. The exposed portion of the Pt core preferentially binds CO and the Cu shell binds O_2, supplying oxygen for the reaction. The Pt–Cu interface provides CO-oxidation sites that are not poisoned by either CO or O_2. Additional computational screening shows that this separation of reactant binding sites is possible for several other core@shell NPs. Our results indicate that the metal–metal interface within a single NP can be optimized for design of bifunctional catalytic systems with improved performance.

Introduction

Pt is an important catalytic material for energy production and conversion.[1] Pt can activate and dissociate molecular oxygen and it has excellent catalytic properties for a number of catalytic reactions including the oxygen reduction reaction (ORR).[2–4] Although the chemical nature of the reactive sites of Pt catalysts is still in many cases debated, the catalytic activity of Pt-based catalysts continues to be a reference point for designing new catalysts.[5]

In many cases, nanoparticle (NP) catalysts are superior to their bulk counterparts. The superior activity of Au NPs for several oxidation reactions clearly shows the potentially unique properties of NP catalysts.[6–10] On the other hand, the low-dimensionality does not always assure the catalytic superiority in Pt catalysts.[11–14] Unlike Au NPs, where the low-dimensional sites are required for facile catalytic reactions,[6–10,15–17] the low-dimensional sites of Pt NPs are regarded less catalytically active due to over-binding of reaction intermediates.[15,18] The well-known ORR activity loss in small Pt NPs has been recognized as a result of the high surface fraction of edge and corner atoms, where the reaction intermediates are over-bound.[11,14,18,19] A similar issue has been raised for CO oxidation where Pt strongly binds CO and thus, easily poisoned.[20]

For catalytic reactions involving CO, such as the CO oxidation reaction ($2CO + O_2 \rightarrow 2CO_2$) and the water–gas shift reaction ($H_2O + CO \rightarrow CO_2 + H_2$), the strong CO-philic nature of Pt plays an important role in the performance of Pt-based catalysts, where CO easily poisons Pt catalysts, blocking the reaction sites and impeding subsequent reaction steps.[20–22] Such CO-poisoning becomes critical when the reaction gas contains both CO and other reactants that interact more weakly with Pt. Even in the case of CeO_2 supported Au NPs, we have reported that CO-poisoning prevents facile CO oxidation.[10] In general, CO-poisoning has been regarded as an unavoidable limitation of Pt NPs (and other metal NPs) for CO-involved catalytic processes.[21,22]

A lot of studies have attempted to overcome the CO-poisoning issue of Pt NPs.[20] The Neurock and Iglesia groups considered the effect of pre-covered CO in the mechanistic study of CO oxidation by studying the CO oxidation pathways available to the CO covered Pt NPs.[20] Multi-component NPs that are relatively free from CO poisoning were suggested by alloying Pt with other metals or forming core@shell NPs.[23–26] Another example is our previous report on the dynamic interface formation strategy which demonstrates the creation of a preferred binding site of O_2 at Au NPs supported on CeO_2.[27]

[a]*Department of Materials Science and Engineering, KAIST, 291-Daehak-ro, Yuseong-gu, Daejeon, 34141 Korea*
[b]*Department of Chemistry and the Institute for Computational Engineering and Sciences, University of Texas at Austin, Austin, TX, USA*
[c]*Department of Materials Science and Engineering, Chungnam National University, 99-Daehak-ro, Yuseong-gu, Daejeon, 34134 Korea. E-mail: kimhy@cnu.ac.kr*
†Electronic supplementary information (ESI) available. See DOI: 10.1039/c7nr01382e
‡These authors have equally contributed to this work.
§Present address: Department of Chemical and Biomolecular Engineering, University of Pennsylvania, Philadelphia, PA, 19104-6315.

A stream of studies for designing Pt-based CO-tolerant CO oxidation catalysts proposed alloys or intermetallic NPs of Pt and early-transition metal elements.[28–33] In these cases, the alloying elements generally provide separate preferential binding sites for O_2.[28,29,31] A set of surface science studies has shown that Cu deposited on Pt films or single crystalline surfaces improves CO-tolerance of Pt.[28,33,34] Yeates and Somorjai[34] and Paffett[33] and coworkers found that Cu sub-monolayers deposited on Pt substrates geometrically block the CO adsorption sites on Pt[34] or weaken the Pt–CO binding through an electronic interaction.[33] Surface deposited Cu generally promotes CO oxidation at the Pt–Cu interface by preferentially interacting with O_2 rather than CO.[28,29] Colen and coworkers found that the Cu sub-monolayer islands formed on Pt(111) were covered with oxygen under CO oxidation conditions while exposed Pt(111) was covered with CO.[28] They suggested that the bifunctional CO oxidation occurs at the Pt–Cu interface.[28]

Moreover, Pt–Cu alloys or intermetallic NPs supported on oxides have been reported as a potential catalyst for CO oxidation or preferential oxidation (PROX) of CO in hydrogen.[29,30,35] In the case of Pt–Cu intermetallic catalysts, Cu was identified as an oxygen supply point[29] consistent with surface science studies. Komatsu and coworkers studied the CO oxidation by PtCu intermetallic NPs supported on Al_2O_3 and SiO_2 and consistently found that Cu has a clear influence on the CO adsorption chemistry of NPs.[29,30] For PtCu NPs supported on Al_2O_3, the Cu sites bind CO more weakly than Pt whereas Cu decorated Pt sites bind CO more strongly than pure Pt.[29] As a result, they suggested the bifunctional CO oxidation reaction at the Pt–Cu interface whose activity can be maximized in regularly ordered PtCu intermetallic NPs.[29]

The observed catalytic performance of bimetallic catalysts is an average function of geometric and electronic effects between comprising elements,[36,37] which are also strongly correlated with synthesis methods. Therefore, it is not easy to extract a specific reactive species which attributes to the improved catalytic performance of bimetallic surfaces or NPs. However, combining two or more elements that independently activate the different reaction stages of the catalytic pathway in a single catalyst system is a highly efficient strategy for designing more consistent catalysts.[27,29,38–47] Bringing a bifunctional nature in catalytic reactions with several consecutive reaction steps has usually improved the selectivity or activity of the reaction.[27,29,38–47]

Here, considering the previous findings of the effectiveness of a bifunctional pathway for the overall performance of heterogeneous catalysts, for example, the activity of Pt or Au NPs supported on CeO_2–TiO_2 mixed oxides,[48,49] facile CO oxidation catalyzed by isolated Cu^+ ions within a framework of TiO_2,[40,42,44] coking resistant CH_4 reforming activated by the Pd/MgO interface,[41] and of course, the above-mentioned previous reports of Pt–Cu surfaces and NPs,[28–30,32–34] we suggest a systematic design strategy for CO-poisoning free Pt-based NPs. Using density functional theory (DFT), we first study the CO-coverage dependent CO and O_2 binding to Pt NPs. Later, we turn to the well-known Pt@Cu NPs to separate the binding sites of CO and O_2 and to target CO oxidation catalysts which are not poisoned by CO. The structure of the Pt@Cu core@shell NPs, which have been synthesized using under potential deposition (UPD)[50] is adopted to study molecular binding at the Pt–Cu interface. A bifunctional CO oxidation pathway at the Pt–Cu interface is found on the Pt NPs covered with a full- or a partial-shell of Cu. Based on the findings of the key factors that initiate the separated binding of CO and O_2 on Pt and Cu, from catalyst design perspectives, we then suggest several other core@shell NPs which can potentially catalyze bifunctional CO oxidation at the interface between two elements and also resist CO-poisoning.

Our results present that atomic-sized metal–metal interfaces within a single NP can be utilized for rational design of advanced catalytic materials with high activity and stability. This is a typical example of a computational catalyst design utilizing a highly reactive and reliable atomically-controlled reaction center.

Computational details

Our Pt NP model consists of 147 Pt atoms in a cuboctahedral structure. Pt_{147}, as the core of the Pt@Cu NPs, has 8 (111) facets and 6 (100) facets. Cu atoms were selectively deposited on the Pt(100) and Pt(111) facets. The full Cu shell covered Pt@Cu model, $Pt@Cu_F$, contains 102 Cu atoms, 6 and 9 on each of the Pt(111) and Pt(100) facets, respectively.[50] We have reported that the UPD of Cu on the Pt NPs proceeds in two sequential steps: Cu deposition on Pt(100) and subsequent Cu deposition on Pt(111).[50] Both the partial (half) shell model with Cu atoms on the Pt(100) facets and the open Pt(111) facets, $Pt@Cu_P$, were considered for these catalytic studies.

In our screening for candidate bifunctional CO oxidation catalysts, various $X_{core}@Y_{shell}$ pairs (X, Y = Ag, Au, Cu, Ir, Pd, Pt, Rh, and Ru) were considered. For these calculations, we used a cuboctahedral Pt_{55} NP with a half shell model (to reduce the computational cost). We show in the ESI† (discussed below) that these core@shell particles all prefer to have their shell on the (100) facets.

We performed spin-polarized DFT calculations using a plane-wave basis with the Vienna *ab initio* simulation package.[51,52] Electronic exchange and correlation were modeled using the PW91 functional.[53] The interaction between the ionic core and the valence electrons was described by the projector augmented wave method.[54] Valence electron wave functions were expanded in a plane-wave basis up to an energy cutoff of 290 eV. The NPs were isolated in a 28 Å cubic cell. The Brillouin zone was sampled at the Γ-point. The convergence criteria for the electronic structure and the atomic geometry were 10^{-4} eV and 0.03 eV $Å^{-1}$, respectively. We used a Gaussian smearing function with a finite temperature width of 0.1 eV in order to improve convergence of states near the Fermi level. Even though the PW91 functional overestimates the Pt–CO binding,[55–57] the magnitude of systematic errors

caused by the functional is not expected to affect our conclusions. The calculation parameters are similar to our previous report,[50] which successfully reproduced experimental catalytic trends.[50,58] The location and energy of transition states (TSs) were calculated with the climbing-image nudged elastic band method.[59,60]

The thermal stability of Pt@Cu NPs at elevated temperatures was evaluated by running constant temperature NVT conventional molecular dynamics (MD) simulations at 300–600 K using the LAMMPS code[61] with the embedded atom method many-body potential. All MD simulations were performed with a time-step of 1 fs, for a total simulation time of 300 ns.

Results and discussion

CO and O_2 adsorption on Pt_{147} NPs

To understand CO and O_2 adsorption on the Pt_{147} NP reference, we calculate the binding energy, E_{bind}, of individual CO and O_2 molecules on each irreducible binding site. Fig. 1a–f show the four binding sites on Pt_{147}: edge, vertex, Pt(100) surface, and the Pt(111) surface, as well as the strongest adsorption geometry of CO and O_2 on each site. CO and O_2 compete for adsorption at all binding sites, but CO binding is always preferred to O_2. Oxygen binds to the Pt(100) surface in two ways: molecular binding and dissociative binding. To quantify the oxygen affinity to the overall surface of Pt_{147} and

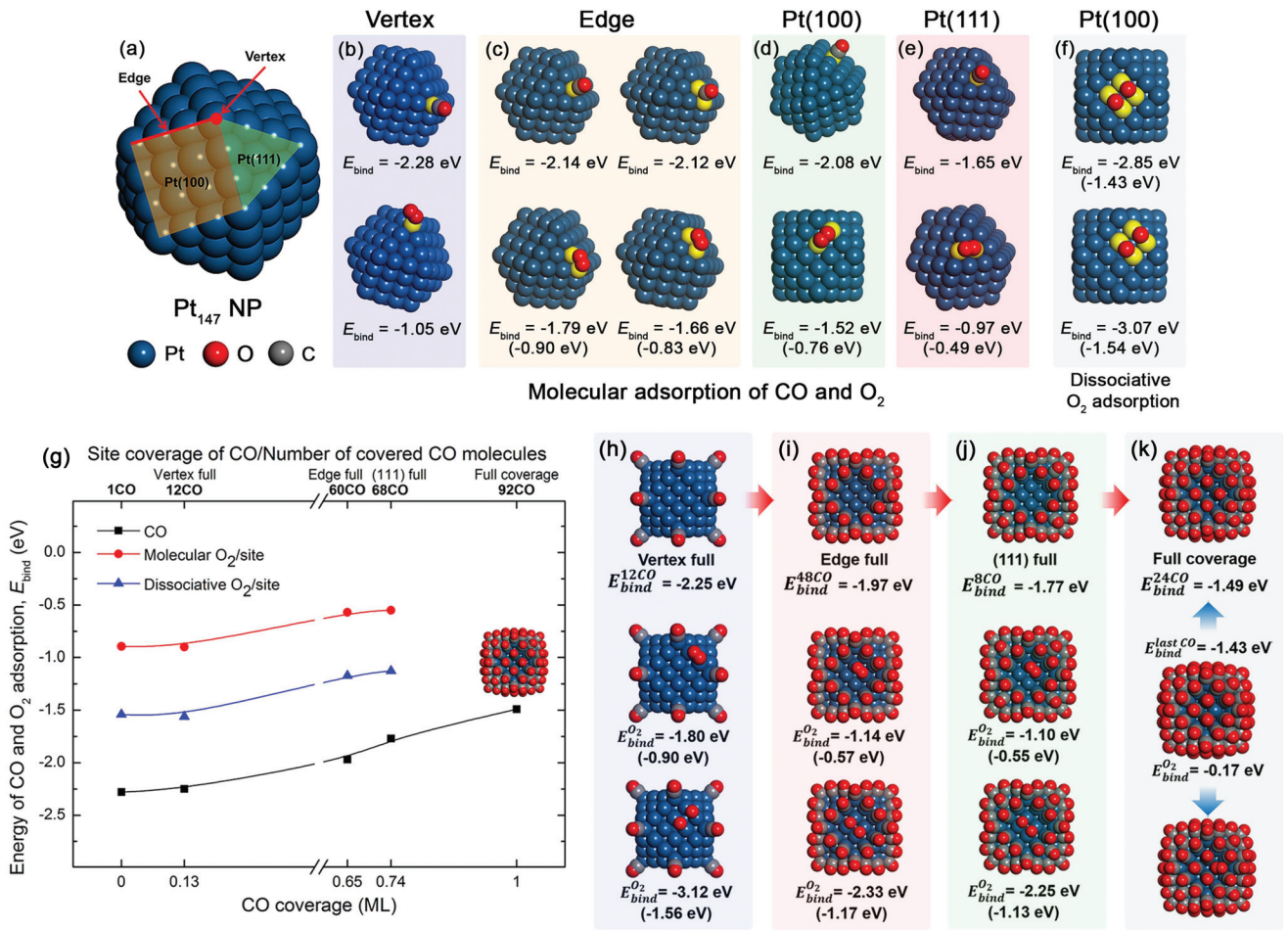

Fig. 1 Adsorption chemistry of Pt_{147} NPs toward CO and O_2. (a) Four binding site categories: Pt(100), Pt(111), edge, and vertex. (b–e). The selected molecular binding geometry of a single CO and O_2 molecule on each site and the corresponding binding energy, E_{bind}. (f) Available dissociative adsorption geometries and the corresponding E_{bind} of O_2 on Pt(100). Because O_2 requires two binding sites, the E_{bind} per single binding site is also presented in the parentheses. Refer to Fig. S1 and S2† for a complete list of CO and O_2 binding geometries. (g) CO coverage dependent change of E_{bind} of CO and O_2. (h)–(k) The average E_{bind} of CO molecules covering the specific binding category and the E_{bind} of molecular and dissociative O_2 adsorption calculated in the presence of differently pre-covered CO molecules. For example, the E_{bind} of O_2 presented in (i) was calculated in the presence of 60 pre-adsorbed CO molecules. E_{bind}^{nCO} in (b)–(e) presents the average E_{bind} of n CO molecules which are filling the corresponding binding category. E_{bind}^{24CO} in (k) represents the average E_{bind} of 24 CO molecules adsorbed on Pt(100). Because the strongest O_2 molecular and dissociative bindings are occurring on Pt(100), we pre-covered the sites on the vertex, edge, and Pt(111) and calculated the E_{bind} of O_2 on Pt(100). The calculated E_{bind} of the first CO, −2.28 eV (b), was decreased down to −1.43 eV for the last binding CO molecule (k). Irrespective of the coverage of pre-covered CO molecules, oxygen binding was always less favorable to the next step of CO binding. The red arrows in (h)–(k) show the preferred binding sequence.

estimate the binding preference of the Pt NP, considering both that the oxygen-binding motif requires two binding sites on Pt whereas CO requires just one site, the calculated E_{bind} (per site) for O_2 is divided by two. For molecular adsorption of CO and O_2 (Fig. 1b–e), the per-site binding of CO is twice that of O_2, confirming the known strong CO-philic nature of Pt. In addition, Pt(100) can dissociatively bind O_2 at the central area of Pt(100) and at the edge-Pt(100) bridging site (Fig. 1f). The per-site binding energy of dissociative O_2 on Pt(100) shows the strongest Pt–O interaction. However, Pt(100) prefers CO binding by 0.65 eV per site which is enough to suppress O_2 coverage on Pt(100) (Fig. 1d and f). A full data set of CO and O_2 binding geometries and energies is presented in the ESI (Fig. S1–S3†).

Under CO oxidation conditions, the NPs are exposed to a mixture of CO and O_2. Although the coverage dependence is an important consideration to understand the state of the catalyst under the reaction conditions, it is rarely considered in theoretical studies due to the high computational cost required to calculate adsorbate binding as a function of surface coverage. Most conventional DFT-based catalysis studies focus on reactants at low coverage. This standard approach is potentially inadequate to address the thermodynamic/kinetic properties of the catalysts under the reaction conditions. Here, to understand the thermodynamics of the CO-poisoning of Pt_{147} NP we calculated the binding energy of CO and O_2 as a function of CO coverage.

Fig. 1g shows the coverage-dependent E_{bind} of CO and of molecularly- or dissociatively-adsorbed O_2 on Pt(100) in the presence of a given number of pre-adsorbed CO molecules. The trend line in Fig. 1g shows that CO binding is thermodynamically preferred to O_2 binding on Pt_{147} NP in the full CO coverage range. For example, the Pt_{147} whose vertex sites bind 12 CO molecules (saturated, Fig. 1h) binds the next 48 CO molecules on its edge sites with an average E_{bind} of −1.97 eV (Fig. 1i) rather than relatively weakly binding O_2 with an E_{bind} of −0.90 eV (molecularly, Fig. 1h) or −1.56 eV (dissociatively, Fig. 1h). Initially, we filled up the strongest CO binding vertex sites first (Fig. 1h), and sequentially filled up the edge (Fig. 1i) and finally the (111) sites (Fig. 1j). Because Pt(100) is the strongest oxygen binding site, we calculated the E_{bind} of O_2 on Pt (100), the strongest O_2 binding case in the presence of pre-adsorbed CO molecules. Moreover, the average CO binding is not significantly different from that of an isolated CO molecule for each site (Table 1).

Interestingly, as in the case reported by the Neurock and Iglesia groups,[20] our calculated sequential E_{bind} of CO molecules predicts that a full coverage of CO (1 ML) is thermodynamically accessible. Even the E_{bind} of the last binding CO was strong enough to suppress O_2 binding (Fig. 1k). Therefore, if unsupported Pt NPs are exposed to the mixture of CO and O_2, a monolayer of CO will cover the surface. Considering that O_2 activation is the key step for facile catalytic CO oxidation, such high coverages of CO would prevent the reaction and lead to CO-poisoning of the Pt_{147} NP.

It is difficult to accurately calculate the lateral repulsive force between the CO molecules adsorbed on Pt NPs by comparing the average E_{bind} of COs because the chemical interaction between the Pt NPs and subsequent CO molecules is affected by pre-adsorbed CO molecules. However, a rough estimate of the CO–CO lateral repulsive forces for each binding category, calculated by comparing the average CO binding and the initial CO binding, shows that the repulsion is not strong enough to hinder the binding of CO molecules at any coverage (Table 1). Even including the entropic contribution to the Gibbs free energy of CO adsorption (0.61 eV), the CO adsorption process would not become endothermic. Similar theoretical results have been reported for Au surfaces: Soto-Verdugo and Metiu reported weak lateral interactions between two CO molecules adsorbed on the Au(111) and Au(100) surfaces (~0.1 eV per CO–CO pair).[62] Our previous results also demonstrate a weak CO–CO lateral interaction on Au–Pd surface alloys (<0.04 eV per CO–CO pair).[47]

Table 1 Comparison of site and coverage dependent E_{bind} of CO of Pt_{147} NPs

	E_{bind} of the first single CO on the corresponding binding site[a]	Average E_{bind} of CO molecules[b]	E_{bind} (ave.-single)[c]
Vertex	−2.28 eV	−2.25 eV (12 CO)	0.03 eV
Edge	−2.11 eV	−1.97 eV (48 CO)	0.14 eV
(111)	−1.81 eV	−1.77 eV (8 CO)	0.04 eV
(100)	−1.60 eV	−1.49 eV (24 CO)	0.11 eV

[a] Calculated in the presence of pre-adsorbed CO molecules. For example, E_{bind} = −2.11 eV of the edge binding CO molecule was calculated by binding one CO molecule on the edge site in the presence of 12 CO molecules bound to the vertex sites. [b] Refer to Fig. 1h–k for geometries. [c] CO–CO lateral repulsive force.

An open surface space for O_2 or OH adsorption, which is essential for facile gas phase CO oxidation or electrochemical CO oxidation catalyzed by Pt NPs, could be secured at elevated temperature[63] or by applying an electrochemical potential,[58] respectively. Dynamic Pt refaceting could also secure a certain level of surface oxygen coverage.[64] More interestingly, we found that the CO–CO repulsive force is emphasized in a small Pt NP supported on CeO_2(111). Even though the size of the model is not compatible with this study, our preliminary results show that the Pt atoms at the Pt–CeO_2 interfacial area cannot be saturated with CO, and thus are potentially available for Pt–O or Pt–O_2 binding (refer to ESI, Fig. S4†).

CO and O_2 adsorption on Pt@Cu NPs

Our CO and O_2 adsorption study shows that a significant portion of the Pt_{147} NP surface binding sites will be occupied by CO, causing CO-poisoning. In our previous report, we studied the sequential structural evolution of Pt@Cu NPs where a monolayer Cu shell was deposited on the Pt_{147} core by UPD.[50] A combination of electrochemical investigations, DFT calculations, and EXAFS analysis confirmed the formation of the $Pt@Cu_F$ NP presented in Fig. 2a.[50]

There are three interesting features of the UPD generated $Pt@Cu_F$ NP: (1) only a monolayer of Cu is deposited on the Pt facets, (2) Cu selectively deposits first on the Pt(100) facet and then on the Pt(111) facet, and (3) even when a full Cu shell is

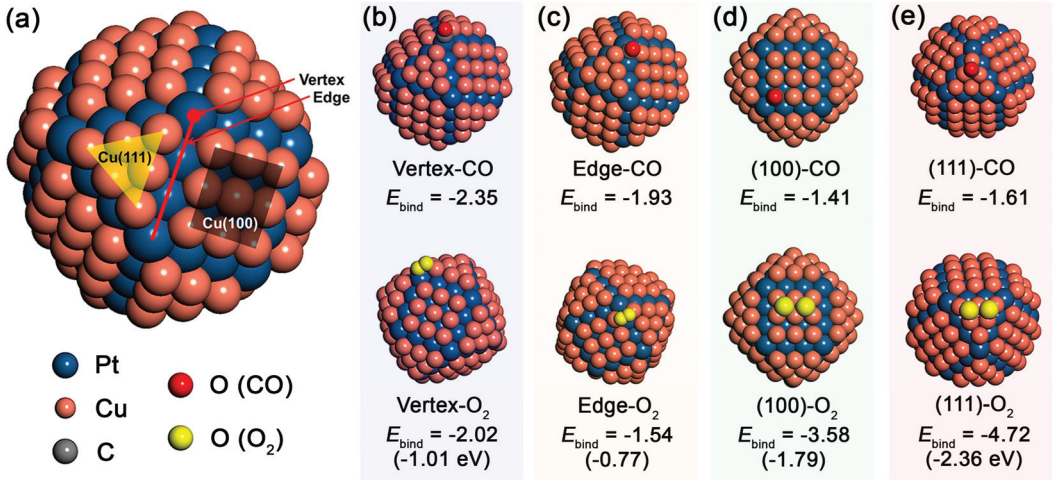

Fig. 2 Adsorption chemistry of Pt@Cu_F NPs toward CO and O_2. (a) Four binding site categories: Cu(100), Cu(111), edge, and vertex. (b–e). The strongest CO and O_2 binding geometry on each site. Refer to Fig. S6 and S7† for a complete list of CO and O_2 binding geometries. For (100)-O_2 and (111)-O_2, dissociatively adsorbed O_2 are presented because the activation barrier of dissociation of molecularly adsorbed O_2 on Cu(100) and Cu(111) was marginally small: 0.01 eV on Cu(111) and 0.16 eV on Cu(100), respectively. Values in the parentheses present the E_{bind} per single Pt binding site.

deposited, open edge and vertex Pt sites remain exposed.[50] Because Cu atoms are selectively deposited on the Pt(100) facets first, the Pt@Cu_P NP structure, with Cu atoms only on the Pt(100) and open Pt(111) facets, could be synthesized.[50]

We start with the idea of bifunctional CO oxidation at the Pt–Cu interface in the Pt@Cu_F NP, where the Cu shell binds and supplies O_2 for oxidation of CO bound to Pt. If the Cu shell preferentially binds O_2 then the Pt@Cu_F NP is intrinsically free from the CO-poisoning. To estimate the binding chemistry of Cu(111), Cu(100), and the Pt vertex and edge sites of Pt@Cu_F, we calculated the E_{bind} of CO and O_2 on each site and show the strongest binding sites in Fig. 2b–e (refer to Fig. S5 and S6† for more binding cases). Clearly, the Cu shell preferentially binds O_2, whereas the Pt vertex and edge sites prefer CO. Therefore, the Pt@Cu_F NP offers spatially separated binding sites for CO and O_2, preventing competition at the same binding site (CO-poisoning). From a catalytic kinetics perspective, having separated binding sites is beneficial for the reaction rate because both reactants are favored to be present on the surface (as discussed below).

The Cu(100) and Cu(111) facets on Pt_{147} show a different oxygen binding trend compared to the Pt_{147} NP. In general, while the Cu facets molecularly bind O_2 (Fig. S6†), low O_2 dissociation barriers (0.01 eV on Cu(111) and 0.18 eV on Cu(100)) indicate that the chemisorbed O_2 will rapidly dissociate into atomic oxygen. As presented in Fig. 2e, Cu(111) binds O_2 more strongly than Cu(100). Additionally, considering the formation of the Cu_2O-like local three-fold Cu–O atomic coordinate,[43] the high −4.72 eV E_{bind} of O_2 (−2.36 eV per O atom) is explained by the formation of CuO_x like species.

Bifunctional CO oxidation by Pt@Cu NPs

To study the CO oxidation mechanism, we initially saturate the open Pt vertex and edge sites of the Pt@Cu_F NPs with CO molecules. Fig. S7† shows that twelve CO molecules can bind to the Pt vertices of Pt@Cu_F, followed by the adsorption of 24 CO molecules on the edge sites. The average binding energy of the 36 CO molecules, E_{bind} = −1.67 eV, is greater (more negative) than the binding energy of O_2 on the edge site (Fig. 2c), confirming that a large portion of exposed Pt sites on Pt@Cu_F will be saturated by CO, as presented in S1 of Fig. 3a and b.

The available CO oxidation pathways activated by an O_2 molecule dissociatively bound on Cu(100) and Cu(111) are presented in Fig. 3a and b. In the presence of 36 pre-adsorbed CO molecules, the Cu(100) and Cu(111) facets strongly bind an O_2 molecule. Because the E_{bind} of O_2 on Cu(100) and Cu(111) is not strongly affected by the presence of the CO molecules, the binding nature of CO and O_2 on Pt@Cu_F presented in Fig. 2 will be conserved under CO oxidation conditions. Since the binding sites of O_2 and CO are separated, the reaction occurs at the Pt–Cu interface.

As briefly discussed above, the Cu shell molecularly binds O_2 and rapidly activates it into dissociated O atoms (Fig. S7c and d†). The dissociation of O_2 on Cu(111) requires a lower activation energy barrier, E_b = 0.01 eV, than on Cu(100), E_b = 0.16 eV (calculated on CO saturated Pt@Cu NPs, Fig. S7c and d†). However, the energy well created by a dissociatively adsorbed O_2 molecule, which is equal to the binding strength of two O atoms on the Cu surface, is almost twice as deep on Cu(111) than on Cu(100). Therefore, the barrier for the next step, CO_2 formation, is higher on Cu(111) (Fig. 3b, TS). The overall landscape of the reaction energetics in Fig. 3a and b suggests that the Pt–Cu(100) interface offers the faster reaction pathway with a lower overall barrier for CO_2 formation than the Pt–Cu(111) interface. Note that we studied the first half of the overall CO oxidation (oxidation of two CO by one O_2) because O_2 activation is generally regarded as the key step for CO oxidation by metallic NPs.[65,66]

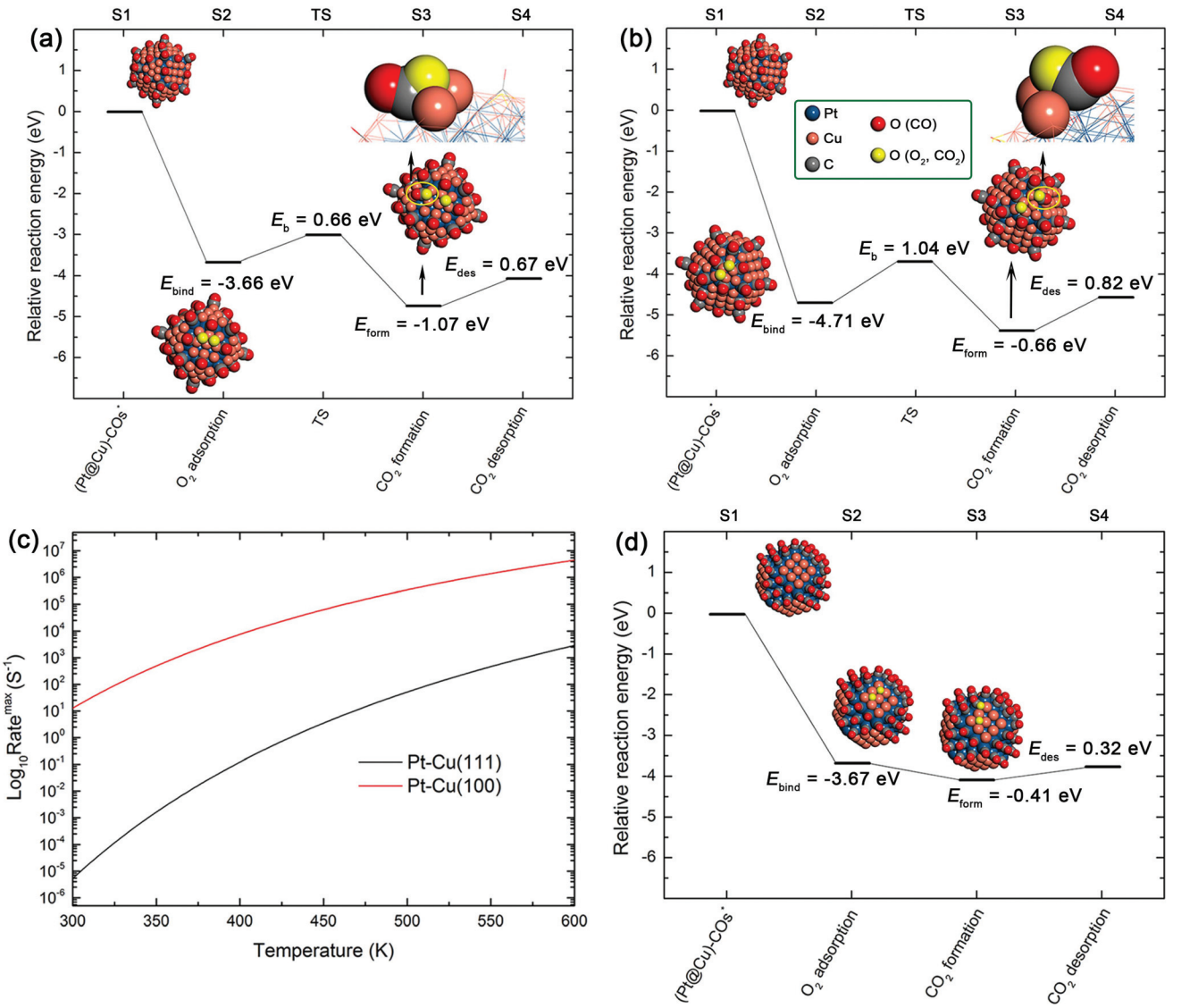

Fig. 3 Bifunctional CO oxidation pathways and the corresponding rate catalyzed by CO-saturated Pt@Cu_F and Pt@Cu_P: (a) CO oxidation by O_2 on Cu(100), (b) reaction by O_2 on Cu(111), and (c) estimated rates of CO oxidation by (a) and (b). Enlarged insets show the morphology of the CO_2-like reaction intermediate formed at the Pt–Cu interface. The Pt–Cu(100) interface offers the faster reaction pathway and higher rate due to a lower energy barrier. (d) Relative location of the energetic states along the bifunctional CO oxidation pathway, catalyzed by CO-saturated Pt@Cu_P. Refer to the ESI† for details of microkinetic modeling.

The rates of CO oxidation at the Pt–Cu(100) and Pt–Cu(111) interfaces of Pt@Cu_F presented in Fig. 3c show that the Pt–Cu(100) interface accounts for the majority of the overall CO oxidation rate by Pt@Cu_F NPs. Even at room temperature the Pt–Cu(100) interface actively catalyzes CO oxidation and the rate rapidly increases as a function of temperature, approaching 10^6 s^{-1} at 600 K (refer to the ESI† for details of microkinetic modeling). Microkinetic modeling shows that the calculated rate of CO oxidation at 300 K is insensitive to fluctuations in p(CO) between 1 bar to 0.01 bar and p(O_2) between 1 bar to 0.21 bar. This result suggests that a Pt@Cu catalyst, which separately binds CO and O_2 on Pt and Cu, can adsorb a constant amount of CO and O_2 under a wide range of reaction conditions. Thus, the catalyst would function even under high CO pressure where conventional Pt NPs would be poisoned by CO. The relative surface concentration of CO and O_2 depends on the surface concentration of Cu and Pt. Therefore, the surface concentration of reacting molecules, which are generally a function of partial pressure, temperature, and ΔE_{bind} of reactants in a single component catalyst,[10] become controllable in our Pt@Cu catalyst. The overall rate becomes a simple function of temperature, allowing for new possibilities in the design of better catalysts.

Pt@Cu_F catalyzes CO oxidation at the Pt–Cu interfacial sites. These sites oxidize CO *via* a local process, similar to the catalysis by single-atom active sites.[17,67] The overall catalytic activity of Pt@Cu would be a direct function of the number of Pt–Cu pairs on the surface of NPs. The size effect on the cata-

lytic activity or the morphology related activity change could be estimated from the structure of Pt@Cu NPs.

Considering the faster CO oxidation at the Pt–Cu(100) interface, we also studied the energetics of CO oxidation by $Pt@Cu_P$, the Pt_{147} NP with a Cu shell on the Pt(100) facets (refer to Fig. 3d and S7†). The $Pt@Cu_P$ was initially fully covered with a total of 68 CO molecules. Because CO oxidation is catalyzed at the local Pt–Cu interfacial sites, the CO molecules on the side opposite to where the activity of $Pt@Cu_P$ was tested were removed for computational efficiency (Fig. S7b†). Fig. 3d presents the energetics of the first CO oxidation at the Pt–Cu(100) interface of $Pt@Cu_P$. The relative energetic location of each state is similar to the case of $Pt@Cu_F$. This again indicates that the catalytic activity of the Pt–Cu interface originated from a local structural motif. As the Cu(100)-like structural confinement is formed on Pt NPs, Cu provides an active site for CO oxidation which is free from CO-poisoning related catalyst deactivation.

Although Cu(111) is regarded as a less active catalyst for CO oxidation than many other noble metals,[68,69] Cu^+ ions are found to be reactive for CO oxidation.[40,42,44,70] In the bulk form, Cu^+ ions in Cu_2O are easily reduced[71] or fully oxidized,[72] and thus deactivated.[73] We have previously reported that Cu^+ ions isolated within a framework of TiO_2 as a $CuTiO_x$ mixed oxide are highly reactive for CO oxidation.[40,42,44] In the case of our Pt@Cu bifunctional catalyst, an electronic analysis shows that Cu(111) and Cu(100) layers are positively charged, and thus slightly oxidized upon deposition on Pt_{147} NPs (Fig. S8b and c†). The Bader charge of Cu(111) and Cu(100) shell atoms corresponds to the 36.2% and 47.6%, respectively, to that of the surface Cu^+ ions of $Cu_2O(111)$ (Fig. S8a†). Although Cu atoms of our Pt@Cu NPs bifunctionally oxidize CO, their intrinsic chemical nature would be close to that of Cu^+ rather than Cu^{2+} or metallic Cu.

Colen *et al.* reported that in their Cu–Pt(111) bimetallic film, the Cu layer was covered with oxygen when the catalyst system was exposed to CO oxidation conditions.[28] However, they showed that these oxygen species could be used for CO oxidation at the Pt–Cu interface by Pt-bound CO molecules.[28] On the other hand, in the case of PtCu intermetallic NPs, Komatsu and coworkers found that PtCu NPs were more reactive for PROX than conventional CO oxidation.[29] The initial CO oxidation activity of PtCu NPs decreased rapidly over time, while the catalyst was consistently reactive for PROX.[29] According to their reaction scheme, hydrogen is required to remove oxygen species on Cu, so the catalyst eventually becomes inactive for conventional CO oxidation without hydrogen.[29] However, considering our positive findings on catalytic CO oxidation by Pt@Cu NPs and previous experimental report by Colen *et al.* on catalytic CO oxidation by Cu deposited on the Pt(111) surface,[28] we hypothesize that the Cu–O binding strength could vary with the dimension of Cu or its local physical/chemical ensemble. The low-dimensional Cu patches on the single crystalline Pt surfaces or the Pt facets of Pt NPs corresponding to Colen's[28] and our case, respectively, could bind oxygen relatively weakly than the Cu atoms of PtCu intermetallic NPs. In a calorimetric study of Cu deposition on Pt(111), Campbell and coworkers reported that the Pt–Cu interaction is stronger than the Cu–Cu interaction.[74] This is natural as Cu can be deposited on the Pt NPs by UPD. Therefore, the chemical potential of Cu on Pt(111) should be lower than the chemical potential of pure Cu.[74] This is also predicted by the electron distribution presented in Fig. S8b and c† showing that Cu atoms of our Pt@Cu NPs were partially oxidized. These pre-oxidized Cu atoms of Pt@Cu would bind an approaching oxygen molecule relatively weakly than pure Cu.[75] Indeed, we found that E_{bind} of a dissociatively bound O_2 on Cu(111) is −6.55 eV, 38.8% stronger than E_{bind} of Pt@Cu (Fig. 2e). These weakly bound oxygen atoms on the Cu atoms of Pt@Cu NPs would oxidize Pt bound CO molecules at the Pt–Cu interface.

On the other hand, according to a study by Komatsu *et al.*, the Pt@Cu catalyst system is likely to lose initial activity for CO oxidation over time. In this case, H_2 addition is expected to regenerate the catalyst, and the catalyst becomes more suitable for PROX than conventional CO oxidation. We are now turning our attention to these more complicated PROX and water–gas shift reaction (CO oxidation by water, $CO + H_2O \rightarrow H_2 + CO_2$) by Pt@Cu NPs. The results will be reported in due course.

For electrochemical CO oxidation, a very recent study reported by the Crooks group experimentally confirmed the presence of atomic sized Cu active sites for electrochemical CO oxidation on their UPD synthesized Pt@Cu NPs with <2% of surface Cu concentration.[58] DFT calculations showed that Cu selectively binds OH and facilitates the bifunctional reaction with CO adsorbed on Pt.[58] The finding that the Cu species on Pt NPs binds and utilize OH for further oxidation steps is promising for the activation of the water–gas shift reaction or PROX, as the utilization of OH is involved in them.

The thermal stability of UPD generated Pt@Cu NPs with various Cu coverages at 350 K were reported in our previous study.[50] We performed expanded MD simulations at various temperature ranges between 300 and 600 K. Temperature dependent structural evolution of $Pt@Cu_F$ NP is presented in Fig. S9.† At lower temperatures of 300 and 400 K, the initial atomic confinement of surface Cu layers was well-maintained. On the other hand, Pt–Cu alloying occurs at higher temperatures between 500 and 600 K, after 300 ns of simulation time. This is natural because the surface energy of Cu is higher than that of Pt.[76] This Cu penetration into the Pt substrate was also reported in the Cu/Pt (111) system by Yeates and Somorjai.[34]

In general, computational approaches assume that the most thermodynamically stable structure of bimetallic NPs, optimized under vacuum, can appear in real catalyst systems. However, when two components of the bimetallic NP interact asymmetrically with reacting molecules, the metal–reactant interaction energy sometimes reverses the thermodynamic stability. For example, Somorjai and coworkers showed that the core and shell elements of Pd (core)@Rh (shell) NPs are reversible under ambient reaction conditions.[77] We also reported that the sub-surface Pd atoms of Au–Pd surface alloys are subject to be segregated to the surface layer under CO oxidation conditions because Pd more strongly binds CO than Au.[47] On the other hand, a recent finding by Divins *et al.*

showed that even the surface atomic arrangement of the bimetallic NPs can be affected by the presence of supporting oxides.[78] These results consistently confirm that the reactive surface species of bimetallic NPs exposed to the reaction conditions could differ from those present in the thermodynamically most stable structure and that such a dynamic effect should be considered for reasonable catalyst design.

An interesting feature of Pt@Cu NPs is that Cu and Pt interact strongly with O_2 and CO, respectively. As shown in Fig. 1, Pt prefers CO to O_2, whereas Cu prefers O_2 to CO (Fig. 2d and e). Because the two comprising elements behave differently under CO oxidation conditions, where the O_2 partial pressure is generally greater than the partial pressure of CO, the driving force for the O_2-driven Cu surface segregation is likely to be stronger than that of the CO-driven Pt surface segregation. As a result, much of the surface Cu atoms of Pt@Cu NPs would survive in the surface layer under CO oxidation conditions.

Screening X@Y NPs for bifunctional CO oxidation

To find more candidates for bifunctional CO-poisoning-free bimetallic catalysts, we extended our idea and tested a total of 56 X@Y core@shell systems. Because our $Pt@Cu_F$ model with 36 CO and one O_2 is comprised of 323 atoms, even conventional GGA-level DFT calculations of this model was computationally demanding. We, therefore, chose a smaller NP model with 55-atoms in a cuboctahedron core and a 24-atom shell on the (100) facets (Fig. S10†). These particles, denoted as $X_{55}@Y_{24}$ NP, (X, Y = Ag, Au, Cu, Ir, Pd, Pt, Rh, or Ru) were computationally screened with respect to their relative CO and O binding energy. For tested $X_{55}@Y_{24}$ NPs, consistent with the case of Pt@Cu NPs, oxygen binding was always more preferred on the (100) facet, (Fig. S10†). To calculate the E_{bind} of O_2 per single binding site, we directly calculated the E_{bind} of atomic oxygen instead of O_2; this quantity is a known descriptor for the CO oxidation activity of NPs.[15] The binding geometries of CO and O at different facets are given in Fig. S11.† We define the preferential segregation energy, $E_{pref} = [E_{bind}(CO) - E_{bind}(O)]_{(100)} - [E_{bind}(CO) - E_{bind}(O)]_{(111)}$, as a measure of the relative binding site preference of CO and O on the $X_{55}@Y_{24}$ NPs. E_{pref} is also an indicator of the CO-poisoning resistance of the X@Y bimetallic NPs. Positive E_{pref} represents the case where the core element binds CO and the shell binds O; negative E_{pref} values indicate that the core element binds O and the shell binds CO.

Fig. 4 presents the matrix of E_{pref} over the 56 tested systems. As we have calculated, the Pt–Cu system is highly resistive to CO-poisoning. Other Pt-core type NPs, including Pt@[Ru,Rh, Pd,Ag], Ir@[Pd,Cu,Ag], [Cu,Ru,Rh,Ag,Au]@Pt, Pd@[Cu,Ag], Ag@Rh and Cu@Au, will also potentially separate the CO and O_2 binding sites. The systems with more earth abundant core elements than Pt, including Pd@[Cu,Ag], Ag@[Pt,Rh], Cu@[Au,Pt], are more promising for practical applications than the Pt, Rh, Au, or Ir core NPs. Moreover, the Pd@Ag, Cu@Au, and Cu@Pt NPs (with relatively small core elements and large shell elements) are thermodynamically more stable than the others, including Pd@Cu and Ag@[Pt,Rh]. On the other hand, the relatively more oxo-philic shell of Pd@Cu and Ag@[Pt,Rh] NPs could offer a high thermal stability by providing an anchoring site to an oxide support.

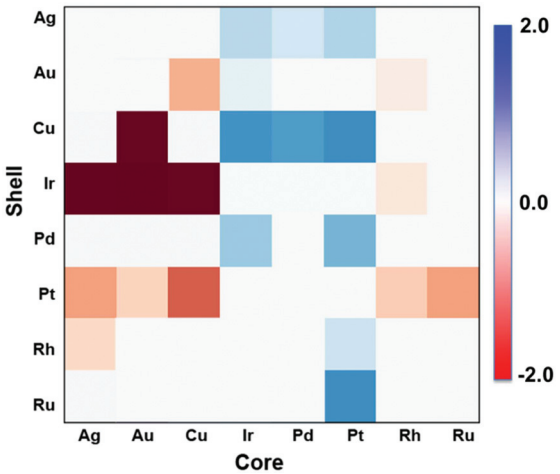

Fig. 4 The preference for CO binding to the shell element and O to the core for 56 X@Y core@shell NPs. Negative (red) indicates that CO binds to the shell and O to the core whereas positive (blue) denotes the reverse case. The chocolate colored systems deformed upon core@shell formation and were not considered in terms of adsorption energetics.

Conclusions

Herein, we demonstrate the computational optimization of NP catalysts with atomically defined reactive sites. The $Pt@Cu_F$ and $Pt@Cu_P$ NPs provide spatially distinct binding sites for CO and O_2. The Pt–Cu interface catalyzes CO oxidation by a bifunctional CO oxidation mechanism; Pt binds CO and Cu supplies oxygen, so that the interface is a CO-poisoning-free active site. Our bifunctional catalyst has a protected site for O_2 activation, and this active site motif can be used to design durable oxidation catalysts. A computational screening suggests other candidates where the metal–metal interface within a single NP can be utilized for poison-free CO oxidation catalysis. In general, combining two or more metallic elements in a single heterogeneous catalyst has been regarded as a method for cost reduction (by reducing the amount of expensive novel metals) or for electronic or structural modification of the hosting material. Our results, however, present that atomic-sized metal–metal interfaces within a single NP can be utilized for rational design of advanced catalytic materials with high activity and stability. As the efficient production of energy and conversion of chemicals is the agenda of heterogeneous catalysis research, our strategy will open up a new avenue for advanced catalyst design.

Acknowledgements

This research was supported by the Basic Science Research Program through the National Research Foundation of Korea

(NRF) funded by the Ministry of Education (NRF-2014R1A1A2057335). This work was conducted under the framework of the research and development program of the Korea Institute of Energy Research (B7-2431). This research used resources of the Center for Functional Nanomaterials, which is a U.S. DOE Office of Science Facility, at Brookhaven National Laboratory under Contract No. DE-SC0012704. The work in Austin was supported by the U.S. Department of Energy, Office of Basic Energy Sciences (DE-FG02-09ER16090) and the Welch Foundation (F-1841). Computing time was provided by the National Energy Research Scientific Computing Center and the Texas Advanced Computing Center at the University of Texas at Austin. Computing time in CNU was provided by the National Institute of Supercomputing and Network/Korea Institute of Science and Technology Information (KSC-2016-C3-0013). We thank Richard M. Crooks for fruitful discussions.

References

1 M. G. Walter, E. L. Warren, J. R. McKone, S. W. Boettcher, Q. Mi, E. A. Santori and N. S. Lewis, *Chem. Rev.*, 2010, **110**, 6446–6473.
2 V. R. Stamenkovic, B. Fowler, B. S. Mun, G. Wang, P. N. Ross, C. A. Lucas and N. M. Marković, *Science*, 2007, **315**, 493–497.
3 J. Kibsgaard, Y. Gorlin, Z. Chen and T. F. Jaramillo, *J. Am. Chem. Soc.*, 2012, **134**, 7758–7765.
4 A. Rabis, P. Rodriguez and T. J. Schmidt, *ACS Catal.*, 2012, **2**, 864–890.
5 J. K. Nørskov, J. Rossmeisl, A. Logadottir, L. Lindqvist, J. R. Kitchin, T. Bligaard and H. Jónsson, *J. Phys. Chem. B*, 2004, **108**, 17886–17892.
6 J. Oliver-Meseguer, J. R. Cabrero-Antonino, I. Domínguez, A. Leyva-Pérez and A. Corma, *Science*, 2012, **338**, 1452–1455.
7 A. S. K. Hashmi, *Science*, 2012, **338**, 1434.
8 A. Wittstock, V. Zielasek, J. Biener, C. M. Friend and M. Bäumer, *Science*, 2010, **327**, 319–322.
9 A. A. Herzing, C. J. Kiely, A. F. Carley, P. Landon and G. J. Hutchings, *Science*, 2008, **321**, 1331–1335.
10 H. Y. Kim, H. M. Lee and G. Henkelman, *J. Am. Chem. Soc.*, 2012, **134**, 1560–1570.
11 M. Shao, A. Peles and K. Shoemaker, *Nano Lett.*, 2011, **11**, 3714–3719.
12 F. Calle-Vallejo, J. Tymoczko, V. Colic, Q. H. Vu, M. D. Pohl, K. Morgenstern, D. Loffreda, P. Sautet, W. Schuhmann and A. S. Bandarenka, *Science*, 2015, **350**, 185–189.
13 K. Ding, A. Gulec, A. M. Johnson, N. M. Schweitzer, G. D. Stucky, L. D. Marks and P. C. Stair, *Science*, 2015, **350**, 189–192.
14 H. A. Gasteiger and N. M. Marković, *Science*, 2009, **324**, 48–49.
15 H. Falsig, B. Hvolbæk, I. S. Kristensen, T. Jiang, T. Bligaard, C. H. Christensen and J. K. Nørskov, *Angew. Chem., Int. Ed.*, 2008, **47**, 4835–4839.
16 J. Saavedra, H. A. Doan, C. J. Pursell, L. C. Grabow and B. D. Chandler, *Science*, 2014, **345**, 1599–1602.
17 Y.-G. Wang, D. Mei, V.-A. Glezakou, J. Li and R. Rousseau, *Nat. Commun.*, 2015, **6**, 6511.
18 K. Kinoshita, *J. Electrochem. Soc.*, 1990, **137**, 845–848.
19 B. C. Han, C. R. Miranda and G. Ceder, *Phys. Rev. B: Condens. Matter*, 2008, **77**, 075410.
20 A. D. Allian, K. Takanabe, K. L. Fujdala, X. Hao, T. J. Truex, J. Cai, C. Buda, M. Neurock and E. Iglesia, *J. Am. Chem. Soc.*, 2011, **133**, 4498–4517.
21 X. Cheng, Z. Shi, N. Glass, L. Zhang, J. Zhang, D. Song, Z.-S. Liu, H. Wang and J. Shen, *J. Power Sources*, 2007, **165**, 739–756.
22 E. Christoffersen, P. Liu, A. Ruban, H. L. Skriver and J. K. Nørskov, *J. Catal.*, 2001, **199**, 123–131.
23 S. Alayoglu, A. U. Nilekar, M. Mavrikakis and B. Eichhorn, *Nat. Mater.*, 2008, **7**, 333–338.
24 Z. Liu, G. S. Jackson and B. W. Eichhorn, *Energy Environ. Sci.*, 2011, **4**, 1900–1903.
25 Y.-C. Hsieh, Y. Zhang, D. Su, V. Volkov, R. Si, L. Wu, Y. Zhu, W. An, P. Liu, P. He, S. Ye, R. R. Adzic and J. X. Wang, *Nat. Commun.*, 2013, **4**, 2466.
26 A. U. Nilekar, S. Alayoglu, B. Eichhorn and M. Mavrikakis, *J. Am. Chem. Soc.*, 2010, **132**, 7418–7428.
27 L. Zhang, H. Y. Kim and G. Henkelman, *J. Phys. Chem. Lett.*, 2013, **4**, 2943–2947.
28 R. E. R. Colen, M. Kolodziejczyk, B. Delmon and J. H. Block, *Surf. Sci.*, 1998, **412–413**, 447–457.
29 T. Komatsu, M. Takasaki, K. Ozawa, S. Furukawa and A. Muramatsu, *J. Phys. Chem. C*, 2013, **117**, 10483–10491.
30 T. Komatsu and A. Tamura, *J. Catal.*, 2008, **258**, 306–314.
31 S. Furukawa, K. Ehara and T. Komatsu, *Catal. Sci. Technol.*, 2016, **6**, 1642–1650.
32 G. Saravanan, R. Khobragade, L. Chand Nagar and N. Labhsetwar, *RSC Adv.*, 2016, **6**, 85634–85642.
33 M. T. Paffett, C. T. Campbell, T. N. Taylor and S. Srinivasan, *Surf. Sci.*, 1985, **154**, 284–302.
34 R. C. Yeates and G. A. Somorjai, *Surf. Sci.*, 1983, **134**, 729–744.
35 T. A. Yamamoto, T. Nakagawa, S. Seino and H. Nitani, *Appl. Catal., A*, 2010, **387**, 195–202.
36 B. Hammer and J. K. Nørskov, *Adv. Catal.*, 2000, **45**, 71–129.
37 F. Gao and D. W. Goodman, *Chem. Soc. Rev.*, 2012, **41**, 8009–8020.
38 M. J. Lee, J. S. Kang, Y. S. Kang, D. Y. Chung, H. Shin, C.-Y. Ahn, S. Park, M.-J. Kim, S. Kim, K.-S. Lee and Y.-E. Sung, *ACS Catal.*, 2016, **6**, 2398–2407.
39 H. Y. Kim, H. M. Lee and J.-N. Park, *J. Phys. Chem. C*, 2010, **114**, 7128–7131.
40 K. Mudiyanselage, S. Luo, H. Y. Kim, X. Yang, A. E. Baber, F. M. Hoffmann, S. Senanayake, J. A. Rodriguez, J. G. Chen and P. Liu, *Catal. Today*, 2016, **263**, 4–10.
41 H. Y. Kim, J. N. Park, G. Henkelman and J. M. Kim, *ChemSusChem*, 2012, **5**, 1474–1481.

42 H. Y. Kim and P. Liu, *J. Phys. Chem. C*, 2015, **119**, 22985–22991.
43 H. Y. Kim and P. Liu, *ChemCatChem*, 2013, **5**, 3673–3679.
44 A. E. Baber, X. Yang, H. Y. Kim, K. Mudiyanselage, M. Soldemo, J. Weissenrieder, S. D. Senanayake, A. Al-Mahboob, J. T. Sadowski and J. Evans, *Angew. Chem., Int. Ed.*, 2014, **53**, 5336.
45 Y. Gorlin and T. F. Jaramillo, *J. Am. Chem. Soc.*, 2010, **132**, 13612–13614.
46 Y. Yan, B. Y. Xia, B. Zhao and X. Wang, *J. Mater. Chem. A*, 2016, **4**, 17587–17603.
47 H. Y. Kim and G. Henkelman, *ACS Catal.*, 2013, **3**, 2541–2546.
48 A. Bruix, J. A. Rodriguez, P. J. Ramírez, S. D. Senanayake, J. Evans, J. B. Park, D. Stacchiola, P. Liu, J. Hrbek and F. Illas, *J. Am. Chem. Soc.*, 2012, **134**, 8968–8974.
49 X. Yang, S. Kattel, S. D. Senanayake, J. A. Boscoboinik, X. Nie, J. Graciani, J. A. Rodriguez, P. Liu, D. J. Stacchiola and J. G. Chen, *J. Am. Chem. Soc.*, 2015, **137**, 10104–10107.
50 E. V. Carino, H. Y. Kim, G. Henkelman and R. M. Crooks, *J. Am. Chem. Soc.*, 2012, **134**, 4153–4162.
51 G. Kresse and J. Furthmüller, *Comput. Mater. Sci.*, 1996, **6**, 15–50.
52 G. Kresse and J. Furthmüller, *Phys. Rev. B: Condens. Matter*, 1996, **54**, 11169–11186.
53 J. P. Perdew and Y. Wang, *Phys. Rev. B: Condens. Matter*, 1992, **45**, 13244–13249.
54 P. E. Blochl, *Phys. Rev. B: Condens. Matter*, 1994, **50**, 17953.
55 L. Schimka, J. Harl, A. Stroppa, A. Grüneis, M. Marsman, F. Mittendorfer and G. Kresse, *Nat. Mater.*, 2010, **9**, 741–744.
56 P. J. Feibelman, B. Hammer, J. K. Nørskov, F. Wagner, M. Scheffler, R. Stumpf, R. Watwe and J. Dumesic, *J. Phys. Chem. B*, 2001, **105**, 4018–4025.
57 B. Hammer, L. B. Hansen and J. K. Nørskov, *Phys. Rev. B: Condens. Matter*, 1999, **59**, 7413–7421.
58 L. Luo, L. Zhang, Z. Duan, A. S. Lapp, G. Henkelman and R. M. Crooks, *ACS Nano*, 2016, **10**, 8760–8769.
59 G. Henkelman and H. Jónsson, *J. Chem. Phys.*, 2000, **113**, 9978–9985.
60 G. Henkelman, B. P. Uberuaga and H. Jónsson, *J. Chem. Phys.*, 2000, **113**, 9901–9904.
61 S. Plimpton, *J. Comput. Phys.*, 1995, **117**, 1–19.
62 V. Soto-Verdugo and H. Metiu, *Surf. Sci.*, 2007, **601**, 5332–5339.
63 N. Guo, B. R. Fingland, W. D. Williams, V. F. Kispersky, J. Jelic, W. N. Delgass, F. H. Ribeiro, R. J. Meyer and J. T. Miller, *Phys. Chem. Chem. Phys.*, 2010, **12**, 5678–5693.
64 S. B. Vendelbo, C. F. Elkjær, H. Falsig, I. Puspitasari, P. Dona, L. Mele, B. Morana, B. J. Nelissen, R. van Rijn, J. F. Creemer, P. J. Kooyman and S. Helveg, *Nat. Mater.*, 2014, **13**, 884–890.
65 H. Y. Kim and G. Henkelman, *J. Phys. Chem. Lett.*, 2012, **3**, 2194–2199.
66 H. Y. Kim, S. S. Han, J. H. Ryu and H. M. Lee, *J. Phys. Chem. C*, 2010, **114**, 3156–3160.
67 C. Du, H. Lin, B. Lin, Z. Ma, T. Hou, J. Tang and Y. Li, *J. Mater. Chem. A*, 2015, **3**, 23113–23119.
68 F. Yang, J. Graciani, J. Evans, P. Liu, J. Hrbek, J. F. Sanz and J. A. Rodriguez, *J. Am. Chem. Soc.*, 2011, **133**, 3444–3451.
69 T. Jiang, D. J. Mowbray, S. Dobrin, H. Falsig, B. Hvolbæk, T. Bligaard and J. K. Nørskov, *J. Phys. Chem. C*, 2009, **113**, 10548–10553.
70 S. Royer and D. Duprez, *ChemCatChem*, 2011, **3**, 24–65.
71 A. E. Baber, F. Xu, F. Dvorak, K. Mudiyanselage, M. Soldemo, J. Weissenrieder, S. D. Senanayake, J. T. Sadowski, J. A. Rodriguez, V. Matolín, M. G. White and D. J. Stacchiola, *J. Am. Chem. Soc.*, 2013, **135**, 16781–16784.
72 G. G. Jernigan and G. A. Somorjai, *J. Catal.*, 1994, **147**, 567–577.
73 T.-J. Huang and D.-H. Tsai, *Catal. Lett.*, 2003, **87**, 173–178.
74 T. E. James, S. L. Hemmingson, J. R. V. Sellers and C. T. Campbell, *Surf. Sci.*, 2017, **657**, 58–62.
75 R. Hoffmann, *Rev. Mod. Phys.*, 1988, **60**, 601–628.
76 A. V. Ruban, H. L. Skriver and J. K. Nørskov, *Phys. Rev. B: Condens. Matter*, 1999, **59**, 15990–16000.
77 F. Tao, M. E. Grass, Y. Zhang, D. R. Butcher, J. R. Renzas, Z. Liu, J. Y. Chung, B. S. Mun, M. Salmeron and G. A. Somorjai, *Science*, 2008, **322**, 932–934.
78 N. J. Divins, I. Angurell, C. Escudero, V. Pérez-Dieste and J. Llorca, *Science*, 2014, **346**, 620–623.